CORA Cork Open Research Archive
Cartlann Taighde Oscailte Chorcaí

Title	Numerical study of a Whitham equation exhibiting both breaking waves and continuous solutions
Authors	Mortell, Michael P.;Mulchrone, Kieran F.
Publication date	2021-04-01
Original Citation	Mortell, M. P. and Mulchrone, K. F. (2021) 'Numerical study of a Whitham equation exhibiting both breaking waves and continuous solutions', AIP Advances, 11 (4), 045002 (13 pp). doi: 10.1063/5.0047582
Type of publication	Article (peer-reviewed)
Link to publisher's version	https://aip.scitation.org/doi/abs/10.1063/5.0047582 - 10.1063/5.0047582
Rights	© 2021 Author(s). All article content, except where otherwise noted, is licensed under a Creative Commons Attribution (CC BY) license (http://creativecommons.org/licenses/by/4.0/). - http://creativecommons.org/licenses/by/4.0/
Download date	2024-04-20 10:22:13
Item downloaded from	https://hdl.handle.net/10468/11182

UCC
University College Cork, Ireland
Coláiste na hOllscoile Corcaigh

AIP Advances

Numerical study of a Whitham equation exhibiting both breaking waves and continuous solutions

Cite as: AIP Advances **11**, 045002 (2021); https://doi.org/10.1063/5.0047582
Submitted: 06 March 2021 . Accepted: 11 March 2021 . Published Online: 01 April 2021

Michael P. Mortell, and Kieran F. Mulchrone

View Online Export Citation CrossMark

ARTICLES YOU MAY BE INTERESTED IN

Comparison study of natural convection between rectangular and triangular enclosures
AIP Advances **11**, 045303 (2021); https://doi.org/10.1063/5.0035007

Nanopatterned metallic transparent electrodes for the near-infrared spectrum
AIP Advances **11**, 045005 (2021); https://doi.org/10.1063/5.0044447

AIP Publishing

© 2021 Author(s).

Numerical study of a Whitham equation exhibiting both breaking waves and continuous solutions

Cite as: AIP Advances 11, 045002 (2021); doi: 10.1063/5.0047582
Submitted: 6 March 2021 • Accepted: 11 March 2021 •
Published Online: 1 April 2021

View Online Export Citation CrossMark

Michael P. Mortell and Kieran F. Mulchrone[a)]

AFFILIATIONS

Department of Applied Mathematics, University College Cork, Cork T12 K8AF, Ireland

[a)]Author to whom correspondence should be addressed: k.mulchrone@ucc.ie

ABSTRACT

We consider a Whitham equation as an alternative for the Korteweg–de Vries (KdV) equation in which the third derivative is replaced by the integral of a kernel, i.e., η_{xxx} in the KdV equation is replaced by $\int_{-\infty}^{\infty} K_\nu(x-\xi)\eta_\xi(\xi,t)d\xi$. The kernel $K_\nu(x)$ satisfies the conditions $\lim_{\nu\to\infty} K_\nu(x) = \delta''(x)$, where $\delta(x)$ is the Dirac delta function and $\lim_{\nu\to 0} K_\nu(x) = 0$. The questions studied here, by means of numerical examples, are whether adjustment of the parameter ν produces both continuous solutions and shocks of the kernel equation and how well they represent KdV solutions and solutions of the underlying hyperbolic system. A typical example is for resonant forced oscillations in a closed shallow water tank governed by the kernel equation, which are compared with those governed by a partial differential equation. The continuous solutions of the kernel equation associated with frequency dispersion in the KdV equations limit to the shocks of the shallow water equations as $\nu \to 0$. Two experimental problems are solved in a single equation. As another example, suitable adjustment of ν in the kernel equation produces solutions reminiscent of a hydraulic and undular bore.

© 2021 Author(s). All article content, except where otherwise noted, is licensed under a Creative Commons Attribution (CC BY) license (http://creativecommons.org/licenses/by/4.0/). https://doi.org/10.1063/5.0047582

I. INTRODUCTION

Shallow water theory is given by the nonlinear equation

$$\eta_t + c_0\eta_x + \frac{2c_0}{h_0}\eta\eta_x = 0, \tag{1}$$

where $\eta = \eta(x,t)$ is the displacement of the fluid surface about the depth h_0 and $c_0 = \sqrt{gh_0}$ is the phase speed. This theory predicts that *all* solutions carrying an increase of elevation break. By wave breaking is meant that the solution remains bounded, but its slope becomes unbounded in finite time. However, observations have established that some shallow water waves do not break, e.g., a solitary wave as observed by Russell in 1844.[1] The Korteweg–de Vries (KdV) equation

$$\eta_t + c_0\left(1 + \frac{3}{2h_0}\eta\right)\eta_x + \gamma\eta_{xxx} = 0, \tag{2}$$

which includes frequency dispersion through the term $\gamma\eta_{xxx}$, with $\gamma = \frac{1}{6}c_0h_0^2$, predicts that no solutions break due to the distinctive steepening and development of infinite gradients well known in nonlinear hyperbolic equations. Also wave breaking initiated by various instabilities is not produced by the KdV equation. However, Brun and Kalisch[2] showed that there is breaking related to spilling at the wave crest. In (2), the total depth from $y = -h_0$ at the bottom to $y = \eta$ at the top is $h(x,t) = h_0 + \eta(x,t)$, and $c_0^2 = gh_0$, where g is the gravitational constant.

The question raised by Whitham[3] was what kind of simpler mathematical equation (other than the governing equations of the water-wave problem or the Euler equations) could include both breaking and continuous solutions. He put forward the model equation

$$\eta_t + \frac{3}{2}\frac{c_0}{h_0}\eta\eta_x + \int_{-\infty}^{\infty} K(x-\xi)\eta_\xi(\xi,t)d\xi = 0, \tag{3}$$

now called the Whitham equation, as a candidate. Here, the kernel

$$K(x) = \frac{1}{2\pi}\int_{-\infty}^{\infty} c(\kappa)e^{ikx}d\kappa, \tag{4}$$

© Author(s) 2021

where $\frac{\omega}{\kappa} = c(\kappa)$ is the phase velocity of the wave with frequency ω. The KdV equation is recovered by the choice

$$K(x) = c_0\delta(x) + \gamma\delta''(x), \tag{5}$$

where $\delta(x)$ is the Dirac delta function; see the work of Lighthill[20] or Erdélyi.[21]

With the choice of $K(x)$ by

$$K(x) = \frac{1}{2}\nu e^{-\nu|x|}, \ \nu = \frac{\pi}{2}, \tag{6}$$

Eq. (3) can describe continuous symmetric waves that propagate unchanged in shape and peak at a critical height (see Fig. 13 of Ref. 4), as well as symmetric waves from an initial triangular pulse input where the forward face near the top steepens and eventually breaks (see Fig 14 of Ref. 4). Seliger[5] had found a sufficient condition for breaking based on an initial asymmetry of the wave, with forward slope greater than the rear slope. The result in Fig. 14[4] shows that the asymmetry is not necessary for breaking. However, the breaking in Fig. 14 seemed to depend on the forward face being steeper than the maximum for the corresponding solitary wave; see Ref. 4. The formal wave-breaking argument of Seliger[5] and Fornberg and Whitham[4] was put on a firm footing in a paper by Constantin and Escher.[6]

The Whitham equation has been the subject of renewed attention in the mathematical community in recent years because of its ability to explain high frequency phenomena in water waves, e.g., it includes the Benjamin–Feir instability, and to justify Whitham's more *ad hoc* methods and conjectures.[7] Ehrnström and Kalisch[8] proved the existence of non-trivial traveling-wave solutions and constructed numerical approximations, while Ehrnström *et al.*[9] proved the existence of and orbital stability of solitary waves. Sanford *et al.*[10] showed that periodic traveling-wave solutions may have modulational stability not previously observed in long-wave models. Moldabayev *et al.*[11] formally derived the Whitham equation from a Hamiltonian principle, thus resolving the "*ad hoc*" nature of the original derivation by Whitham. Hur and Johnson[12] proved the modulational instability of the linearized periodic wave solution. Carter[13] determined how accurately the bidirectional Whitham equation models the output of the experiments of Hammack and Segur[14] for long waves on shallow water. His conclusion is that the unidirectional Whitham equation, including surface tension, provides the most accurate predictions for these experiments. Hur[15] proved wave breaking in the Whitham equation, provided that the slope of the initial data is sufficiently negative, where the phase speed $c(\xi)$ is $c(\xi)^2 = \frac{\tanh\xi}{\xi}$, and this result is generalized in Ref. 16. It is shown in Ref. 2 that for solitary or cnoidal solutions of the KdV equation, where for critical amplitudes the particle velocity exceeds the phase velocity near the crest of the wave, incipient wave breaking occurs. Ehrnström and Wahlén[17] settled Whitham's conjecture about the highest cusp on a peaked wave. The comparison of the numerical solutions of the Whitham equation to the numerical approximations of solutions of the full Euler free-surface water-wave problem, where the phase speed is $c(\kappa)^2 = \frac{g}{\kappa}\tanh\kappa h_0$, is given in Ref. 18.

Our purpose here is to numerically examine a model equation, such as Eq. (3) with $K = K_\nu$, where the kernel $K_\nu(x)$, given by (11), has an arbitrary parameter ν such that as $\nu \to \infty$, we recover the KdV equation and as $\nu \to 0$, we obtain the shallow water equation. The parameter ν controls the relative strength of the dispersive effect and the breaking effect. By adjusting ν, we can observe how continuous solutions of the KdV yield to become shocks of shallow water theory.[22]

This paper proceeds by a series of numerical examples after the kernel $K_\nu(x)$ has been introduced and solutions of the kernel equation have been compared with the KdV for exact one-soliton and two-soliton solutions for various values of the parameter ν. Figures 7 and 8 show the breaking of a soliton with a decrease in ν. Section IV is concerned with periodically forced KdV equations and kernel equations for resonant and off-resonant forcing. The kernel equation yields continuous solutions for the forced KdV and shocks for shallow water theory. Thus, the results of two independent experiments are contained in the kernel equation. Section V treats resonant oscillations of a forced *modified* KdV equation. Finally, we show a simple mathematical model whose solutions resemble undular and hydraulic bores and are controlled by the parameter ν.

II. A KERNEL FOR THE WHITHAM EQUATION $K_\nu(x)$: CONSTRUCTION AND TESTING

The background to (3) and (4) is as follows: Whitham was interested in finding a simpler equation that can capture the breaking effect of water waves as in hyperbolic equations. He proposed (3) and (4), where c is given by (7). However, this equation was not easy to deal with, and then, he approximated the kernel by (6). This kernel is the Green's function for the operator $\frac{d}{dx^2} - \nu^2$. The kernel

$$\frac{\omega}{\kappa} = c(\kappa) = \sqrt{\frac{g\tanh h_0\kappa}{\kappa}} \tag{7}$$

is the dispersion relation for water of arbitrary depth h_0. This form combines full linear dispersion with long-wave nonlinearity and has been the subject of much recent research; see Sec. I. When incorporated into Eq. (3), then (3) is often referred to as the Whitham equation.

A. Construction

Whitham's idea of replacing the dispersive term η_{xxx} in the KdV by $\int_{-\infty}^{\infty} K(x-\xi)\eta_\xi(\xi,t)d\xi$ allows the construction of a more general dispersion term that can be used to "soften" the effect of the KdV dispersion and allow for greater influence of the nonlinear term $\eta\eta_x$.

We follow the definition of a "generalized" function by means of a sequence, as in Ref. 20. We begin with the observation that

$$\eta_{xxx} \equiv \int_{-\infty}^{\infty}\delta''(x)\eta_\xi d\xi, \tag{8}$$

and by comparison with the kernel term in Eq. (3), we are motivated to seek a function that approximates $\delta(x)$ and use its second derivative as the kernel. To this end, we chose a Gaussian function $f(x) = ae^{-bx^2}$. We require $\int_{-\infty}^{\infty} f(x)dx \equiv 1 \Rightarrow b = \pi a^2$ to match a key property of $\delta(x)$. Choosing $a = \frac{\nu^2}{\sqrt{\pi}}$ gives

$$f(x) = \frac{\nu^2}{\sqrt{\pi}}e^{-\nu^4x^2}, \ -\infty < x < \infty. \tag{9}$$

© Author(s) 2021

We note that $f(x)$ is a "good" function (see Ref. 20) since $f(x)$ is differentiable for all x any number of times and $f(x)$ and all its derivatives are $\mathcal{O}(|x|^{-N})$ as $x \to \infty$ for all N. We note the following properties of $f(x)$:

1. $\int_{-\infty}^{\infty} f(x)dx = 1$, i.e., $f(x)$ has zero mean,
2. $f(x)$ has a maximum at $x = 0$ with value $f(0) = \frac{\nu^2}{\sqrt{\pi}}$ and $f(0) \to \infty$ as $\nu \to \infty$, and
3. the Gaussian $\mathcal{N}(0, \frac{1}{\sqrt{2}\nu^2}) = f(x)$ and the variance $\frac{1}{\sqrt{2}\nu^2} \to 0$ as $\nu \to \infty$.

The sequence $g_n(x) = \frac{n^2}{\sqrt{\pi}} e^{-n^4x^2}$ with $\int_{-\infty}^{\infty} g_n(x)dx = 1$ is regular, and $\lim_{n\to\infty} g_n(x)F(x)dx$ exists for any good function $F(x)$; see Ref. 20.

Theorem II.1. *The sequence* $\frac{n^2}{\sqrt{\pi}} e^{-n^4x^2}$ *defines a generalized function* $\delta(x)$ *such that* $\int_{-\infty}^{\infty} \delta(x)F(x)dx = F(0)$, *where* $F(x)$ *is a good function. The proof sketched here follows the work of Lighthill,*[20]

$$\frac{n^2}{\sqrt{\pi}} \int_{-\infty}^{\infty} |x| e^{-n^4x^2} dx = \frac{1}{\sqrt{\pi}n^2}.$$

Then, we have

$$\left| \int_{-\infty}^{\infty} \frac{n^2}{\sqrt{\pi}} e^{-n^4x^2} F(x)dx - F(0) \right| = \left| \int_{-\infty}^{\infty} \frac{n^2}{\sqrt{\pi}} e^{-n^4x^2} (F(x) - F(0))dx \right|,$$

$$\leq \max|F'(x)| \int_{-\infty}^{\infty} \frac{n^2}{\sqrt{\pi}} e^{-n^4x^2} |x|dx$$

$$= \frac{\max|F'(x)|}{\sqrt{\pi}n^2} \to 0 \text{ as } n \to \infty.$$

Now, $\frac{\nu^2}{\sqrt{\pi}} e^{-\nu^4x^2}$ is "equivalent" to $\frac{n^2}{\sqrt{\pi}} e^{-n^4x^2}$ (see Ref. 20); therefore,

$$\lim_{\nu\to\infty} \frac{\nu^2}{\sqrt{\pi}} e^{-\nu^4x^2} = \delta(x). \tag{10}$$

Our proposed kernel is derived by taking the second derivative of $\delta(x)$ in (10) and is defined as

$$K_\nu(x) = 2\frac{\nu^6}{\sqrt{\pi}}(2\nu^4x^2 - 1)e^{-\nu^4x^2} \tag{11}$$

(see Fig. 1) with a corresponding expression for $c(\kappa)$, the inversion of (4),

$$c(\kappa) = \int_{-\infty}^{\infty} K_\nu(x)e^{-i\kappa x}dx = -\kappa^2 e^{-\frac{\kappa^2}{4\nu^4}}. \tag{12}$$

In summary, $f(x) = \delta(x)$ as $\nu \to \infty$. For $\nu \ll \infty$, it exhibits a bell-shape and is thus a "softer" version of $\delta(x)$. For $\nu = 0$, we have $K_\nu(x) = 0$ so that our approximation for η_{xxx} [e.g., in Eq. (3)] also becomes 0. In other words, as $\nu \to 0$, the KdV becomes the shallow water theory.

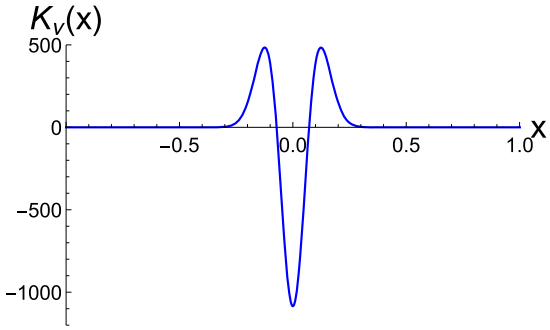

FIG. 1. Plot of $K_\nu(x)$ vs x for $\nu = \pi$.

$K_\nu(x)$ has a large negative peak at $x = 0$ for $\nu = \pi$. In comparison, the peaks for $\frac{1}{2}\pi$ and $\frac{1}{4}\pi$ are negligible, showing that the dispersion effect is being diminished in the KdV equation, thus allowing the breaking of a wave controlled by the nonlinear term $\eta\eta_x$. We note that $\max\left|K_{\frac{\pi}{2}}(x)\right| = o(\max|K_\pi(x)|)$ and $\max\left|K_{\frac{\pi}{4}}(x)\right| = o\left(\max\left|K_{\frac{\pi}{2}}(x)\right|\right)$.

B. Numerical methods

Most of the equations numerically solved here have the form

$$\eta_t + \gamma\eta\eta_x + \int_{-\infty}^{\infty} K(x-\xi)\eta_\xi(\xi,t)d\xi = F(x), \tag{13}$$

where $F(x)$ is a forcing term, which may or may not be zero, and γ is some number. We employ a pseudospectral method to solve these equations (see Refs. 4, 24, and 25). From Fourier analysis, we have that

$$\mathcal{F}\left[\frac{\partial^n \eta}{\partial x^n}\right] = (i\kappa)^n \mathcal{F}[\eta(x)],$$

where $\mathcal{F}$ is the Fourier transform. Thus, the term $\gamma\eta\eta_x$ can be written as $\gamma\eta\mathcal{F}^{-1}[i\kappa\mathcal{F}[\eta]]$. Furthermore, $K(x) = \mathcal{F}^{-1}[c(\kappa)]$ and $c(\kappa) = \mathcal{F}[K(x)]$. Making use of the convolution theorem

$$\int_{-\infty}^{\infty} K(x-\xi)\eta_\xi d\xi = \mathcal{F}^{-1}[i\kappa c(\kappa)\mathcal{F}[\eta]],$$

we can now write Eq. (13) as

$$\eta_t + \gamma\eta\mathcal{F}^{-1}[i\kappa\mathcal{F}[\eta]] + \mathcal{F}^{-1}[i\kappa c(\kappa)\mathcal{F}[\eta]] = F(x). \tag{14}$$

This equation is readily solved by employing discrete versions of the Fourier transform combined with standard solvers for ordinary differential equations. In particular, the Matlab ode45 routine is used, which is a type of Runge–Kutta method and implements the Dormand–Prince (RKDP) method.[19] It should be noted that it is an implicit assumption of the technique that the boundary conditions are periodic in space.

We are also interested in solving for the steady state solution of Eq. (13) when $F(x) \neq 0$. The equation becomes

$$\gamma\eta\eta_x + \int_{-\infty}^{\infty} K(x-\xi)\eta_\xi(\xi,t)d\xi = F(x) \tag{15}$$

© Author(s) 2021

and is solved by taking a Fourier series approximation of η as follows:

$$\eta \approx \sum_{j=-N}^{N} c_j e^{ijmt},$$

where m is assumed to be the frequency of the forcing term. Taking derivatives and substituting these expressions into Eq. (15) and tidying up, we produce a set of nonlinear equations for the unknown coefficients c_j. Taking all coefficients to be initially zero, the solution is found numerically.

C. Numerical test of validity against one-soliton and two-soliton exact solutions

In this section, we demonstrate numerically that the KdV with the kernel $K_\nu(x)$, given by Eq. (11), produces accurate results for large enough ν by comparing the numerical solutions of the $K_\nu(x)$ equations with exact solutions of the KdV. Two cases are considered:

1. One soliton. The equation to be solved is

$$\eta_t + \frac{3}{2}\eta\eta_x + \eta_{xxx} = 0 \tag{16}$$

with initial condition $\eta(x,0) = 2\text{sech}^2(\frac{1}{2}x)$. The factor $\frac{3}{2}$ is that for water, and the exact solution is $\eta(x,t) = 2\text{sech}^2(\frac{1}{2}(x-t))$; see Ref. 3. The corresponding kernel equation to be solved numerically is

$$\eta_t + \frac{3}{2}\eta\eta_x + \int_{-\infty}^{\infty} K_\nu(x-\xi)\eta_\xi(\xi,t)d\xi = 0. \tag{17}$$

2. Two soliton. The equation to be solved is

$$\eta_t - 6\eta\eta_x + \eta_{xxx} = 0 \tag{18}$$

with initial condition $\eta(x,0) = -6\,\text{sech}^2 x$. The exact solution is

$$\eta(x,t) = -\frac{12(\cosh(64t-4x) + 4\cosh(8t-2x) + 3)}{(\cosh(36t-3x) + 3\cosh(28t-x))^2},$$

see Ref. 26, i.e., one-soliton traveling with speed 4 and the other with speed 16. The corresponding kernel equation to be solved numerically is

$$\eta_t - 6\eta\eta_x + \int_{-\infty}^{\infty} K_\nu(x-\xi)\eta_\xi(\xi,t)d\xi = 0. \tag{19}$$

The exact and numerical solutions are compared using the mean squared error of their difference. Denote the numerical solution by $\hat{\eta}(x_i,t_j)$, where x_i are discrete points in the space domain where the solution is calculated. For a domain of length L with N equally spaced nodes, then $x_i = -\frac{L}{2} + i\Delta x$, where $i = 0,\ldots,N-1$. Similarly, t_j are the discrete points in time where the numerical solution is calculated, and for a time step Δt, then $t_j = j\Delta t$, where j goes from 0 to the total number of time steps. The mean squared error, $E(t_j)$, at a particular time t_j is then given by

$$E(t_j) = \frac{1}{N}\Sigma_{i=0}^{N-1}(\eta(x_i,t_j) - \hat{\eta}(x_i,t_j))^2. \tag{20}$$

The results are summarized in Fig. 2. In the case of one soliton, the numerical solution was run until $t = 200$. The error is $< 10^{-3}$ for $\nu \geq \frac{3}{4}\pi$. As the value of ν increases up to 2π, the error drops below 10^{-7} [see Fig. 2(a)]. An example plot, comparing the exact and numerical solutions, is shown in Fig. 2(b) at $t = 200$ and $\nu = 2\pi$,

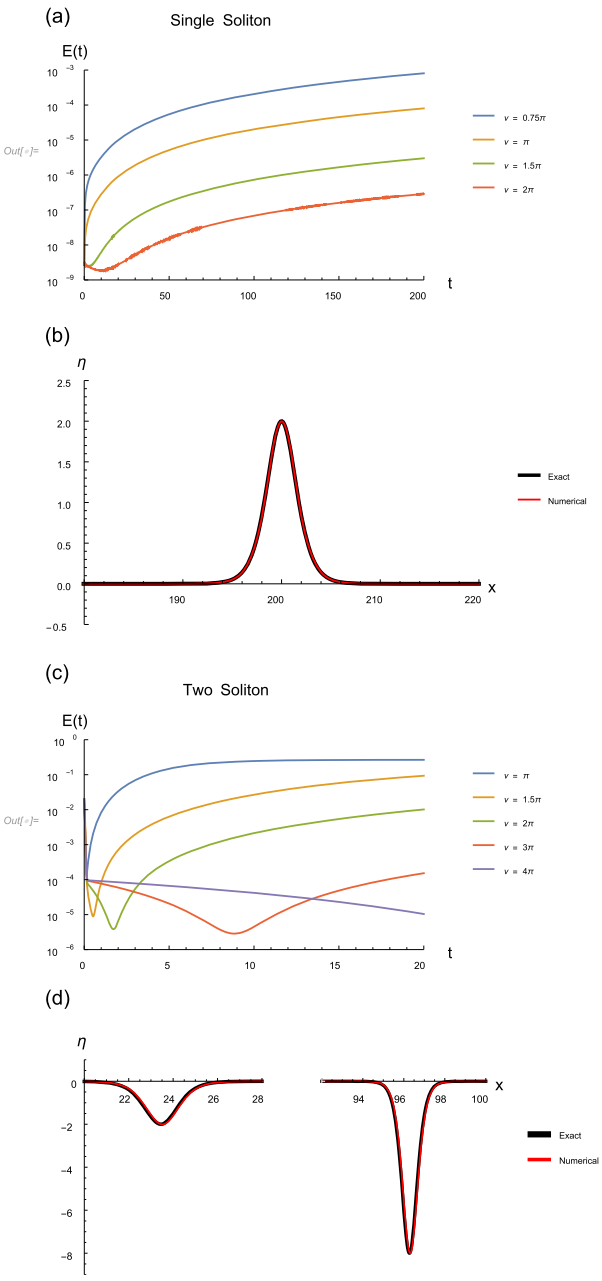

FIG. 2. Plots of the error of numerical solutions for the one-soliton and two-soliton problems (note logarithmic scale) and a comparison of the exact and numerical solutions at specific times. (a) One-soliton error $E(t)$. (b) One-soliton exact and numerical solution at $t = 200$ and $\nu = 2\pi$. (c) Two-soliton error $E(t)$, $0 \leq t \leq 20$. (d) Two-soliton exact and numerical solution at $t = 6$ and $\nu = 2\pi$, zooming in on soliton positions.

© Author(s) 2021

and because the error is very small, no difference can be seen. If the value of ν drops lower than $\sim\frac{3}{4}\pi$, then the equation becomes dominated by shallow water theory and shocks develop. To cope with shocks numerically, a Burgers term (i.e., $\varepsilon\eta_{xx}$ for $0 < \varepsilon \ll 1$) would need to be introduced. However, this means that we are solving a different equation and the comparison with the exact solution is no longer valid. Note that the single soliton numerical solution was studied for different time steps and spatial resolutions and a summary is provided in an electronic appendix. It was found that the method is robust, but the errors may be slightly larger or smaller.

Working with the two-soliton solution requires more care because (i) the solution immediately splits into two distinct solitons, one of height ≈ -2 traveling slowly to the right and another of height ≈ -8 traveling rapidly to the right [see Fig. 2(d)]. This means that for modest time values, the space domain required to capture the solution becomes quite large. (ii) The exact solution becomes numerically intractable at large values of $|x|$ due to the presence of the cosh function. Theoretically, at large $|x|$, i.e., far from the peaks, the exact solution is 0. However, calculating it numerically involves finding the ratio of two very large numbers, which leads to overflow. For this reason, the error in the two-soliton solution is only studied up to $t = 6$ directly from the exact solution. The error associated with the numerical solution is $< 10^{-1}$ for $\nu \geq \pi$, but for $\nu > 2\pi$, the error becomes $\sim< 10^{-2}$ [see Fig. 2(c)]. A visual comparison between a numerical and an exact solution when $\nu = 2\pi$ and $t = 6$ is shown in Fig. 2(d), and no difference is evident. Once more, as in the single soliton case, reducing $\nu < \pi$ introduces shocks.

Figure 2(d) gives the comparison between the exact and numerical solutions for $t = 6$ for Eq. (18). To compare the error for larger times [i.e., up to $t = 20$ in Fig. 2(c)], the two-soliton solution is replaced by a pair of solitary solutions. The solitary wave solutions to Eq. (18) are

$$\eta(x,t) = -8\mathrm{sech}^2\left(2(x-16t) - \frac{1}{2}\ln 3\right) \tag{21}$$

and

$$\eta(x,t) = -2\mathrm{sech}^2\left(x - 4t + \frac{1}{2}\ln 3\right). \tag{22}$$

The occurrence of $\frac{1}{2}\ln 3$ in Eqs. (21) and (22) is a consequence of the interaction of the pulses prior to $t = 1$. The larger pulse is moved forward by an amount $\frac{1}{2}\ln 3$ relative to where it would have been if there was no interaction, while the smaller pulse is retarded by the same amount $\frac{1}{2}\ln 3$. Once the interaction has taken place, the solution of Eq. (18) is the superposition of single soliton waves (21) and (22). The error graph is given in Fig. 2(c) for $0 \leq t \leq 20$. We note that (18) reduces to (16) with the change of variable $\eta = -\frac{1}{4}\hat{\eta}$.

The purpose here is to have exact solutions as the benchmark and to measure the accuracy of approximation (17) against this standard. The larger the parameter ν, the more accurate the approximation for a longer time, which is seen in Sec. IV to include the time to generate a periodic solution. Figures 2(a) and 2(c) demonstrate that the accuracy decreases over time even for larger ν.

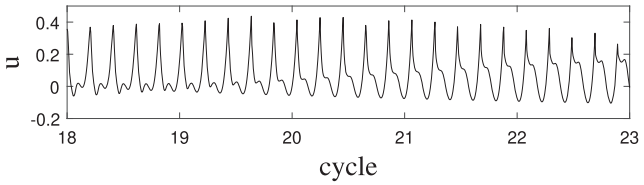

FIG. 3. Time evolution of Eqs. (23) and (24) using the kernel $K(x) = \frac{1}{2}\nu e^{-\nu|x|}$ of Fornberg and Whitham,[4] $\varepsilon = 0.0005$, and $\nu = \frac{\pi}{2}$. The initial condition is a series of five equally spaced triangular pulses of 1.6 base width and 0.48 height. A line plot for 18–23 cycles corresponds to a waterfall plot as in Ref. 4. The top of the forward face steepens and shocks appear. A cycle is defined to be a single linear transect from left to right through the spatiotemporal domain with time progressing by a specified amount. For example, in a cycle, here x goes from −15 to 15 and time progresses by 1 s.

III. APPLICATION TO THE KORTEWEG–DE VRIES EQUATION

Fornberg and Whitham[4] considered the equation

$$u_t + \frac{3}{2}uu_x + \int_{-\infty}^{\infty} K(x-\xi)u_\xi(\xi,t)d\xi = \varepsilon u_{xx}, \tag{23}$$

with

$$K(x) = \frac{1}{2}\nu e^{-\nu|x|}, \quad \nu = \frac{1}{2}\pi, \quad 0 < \varepsilon \ll 1, \tag{24}$$

to investigate if forward breaking, typical of shallow water theory, is possible. They took as the initial condition a symmetrical triangular shape of 0.48 height and 1.6 base width. The result was that the forward face near the top steepens and eventually breaks (see Fig. 14

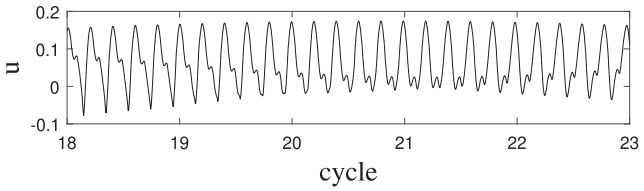

FIG. 4. Continuous solution, time evolution of Eq. (23), $\nu = \frac{\pi}{4}$, and $\varepsilon = 0.005$ with kernel $K_\nu(x)$ given by Eq. (11). The initial condition is a series of five equally spaced triangular pulses of 1.6 base width and 0.48 height. A line plot for 18–23 cycles (compare with Fig. 3).

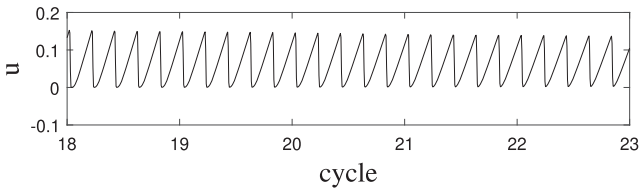

FIG. 5. Shocks, time evolution of Eq. (23), $\nu = \frac{\pi}{8}$, and $\varepsilon = 0.005$ with kernel $K_\nu(x)$ given by Eq. (11). The initial condition is a series of five equally spaced triangular pulses of 1.6 base width and 0.48 height. A line plot for 18–23 cycles (compare with Fig. 3), where shocks are evident and the result is a saw-tooth wave.

© Author(s) 2021

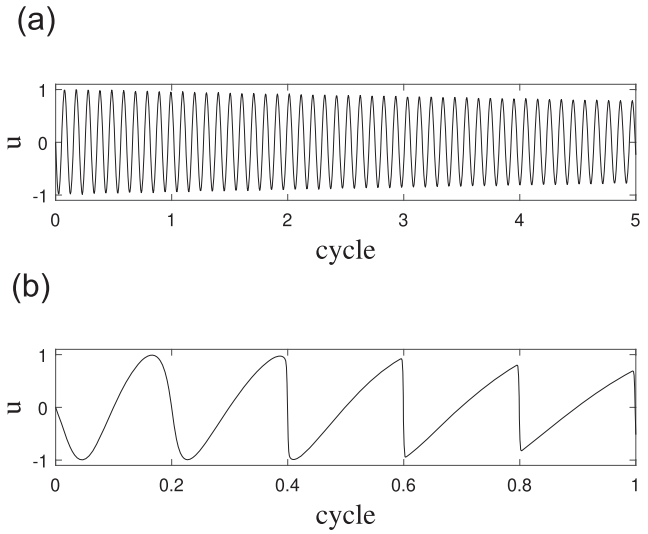

FIG. 6. Time evolution of Eq. (25), $\varepsilon = 0.005$ with kernel $K_\nu(x)$. The initial condition is $u(x,0) = \sin \pi x$. (a) Line plot of time evolution, $\nu = \pi$, for the first five cycles. The solution is smooth and continuous with slow decay. (b) Line plot of time evolution, $\nu = \frac{\pi}{4}$, for the first cycle. This demonstrates that the solution rapidly evolves from a continuous to a shock solution. There is then decay due to the shock.

of Ref. 4, and see also the line plot in Fig. 3 here). They noted that the velocity of the crest was ~0.75 and fits with shallow water theory, which gives a value of 0.72. The wave breaks at $t = 1.0$. The term εu_{xx} in Eq. (23) ensures that the breaking can be replaced by a thin layer.

We now replace $K(x)$ in Eq. (23) with $K_\nu(x)$ defined in Eq. (11), $\varepsilon = 0.005$, and the triangular initial condition remains the same. The outputs are shown in Fig. 4 for $\nu = \frac{\pi}{4}$ and in Fig. 5 for $\nu = \frac{\pi}{8}$. For $\nu = \frac{\pi}{4}$, the output is continuous, which contrasts with that of Fornberg and Whitham[4] (Fig. 14), while the solution for $\nu = \frac{\pi}{8}$ in Fig. 5 contains shocks. Thus, the solutions of Eq. (23) with $K(x) = K_\nu(x)$ can be tuned to be continuous or discontinuous using the parameter ν.

As a further example, we consider Eq. (23) with $K(x) = K_\nu(x)$ and $\frac{3}{2}$ replaced by 1 for $\nu = \pi$ and $\frac{\pi}{4}$, i.e.,

$$u_t + uu_x + \int_{-\infty}^{\infty} K_\nu(x-\xi) u_\xi(\xi,t)\, d\xi = \varepsilon u_{xx} \tag{25}$$

for $0 < \varepsilon \ll 1$ with initial condition

$$u(x,0) = \sin \pi x, \tag{26}$$

and a Burgers term εu_{xx} is included so that a shock is replaced by a sharp but smooth transition.

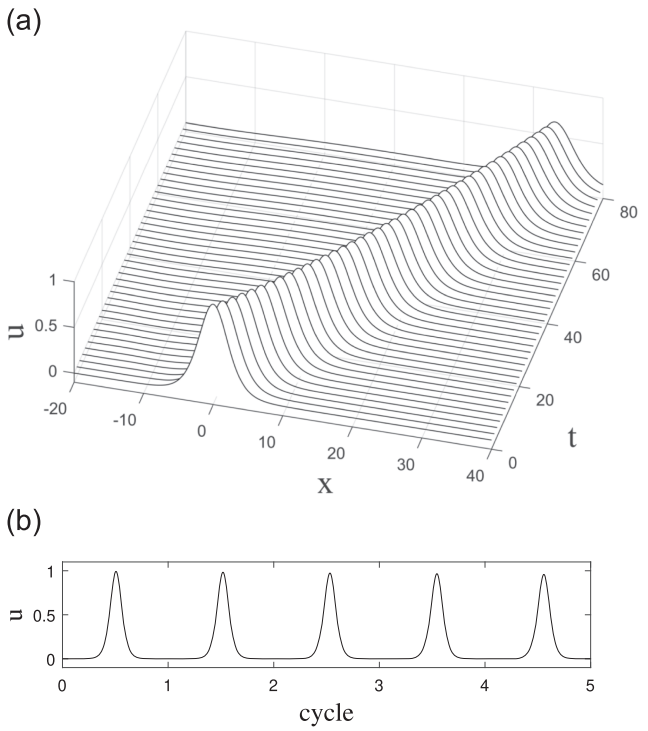

FIG. 7. Plots of the time evolution of Eq. (23), $\varepsilon = 0.05$ with kernel $K_\nu(x)$. The initial condition is given by Eq. (27). (a) $\nu = \pi$. The solution is smooth and continuous. (b) Line plot corresponding to (a).

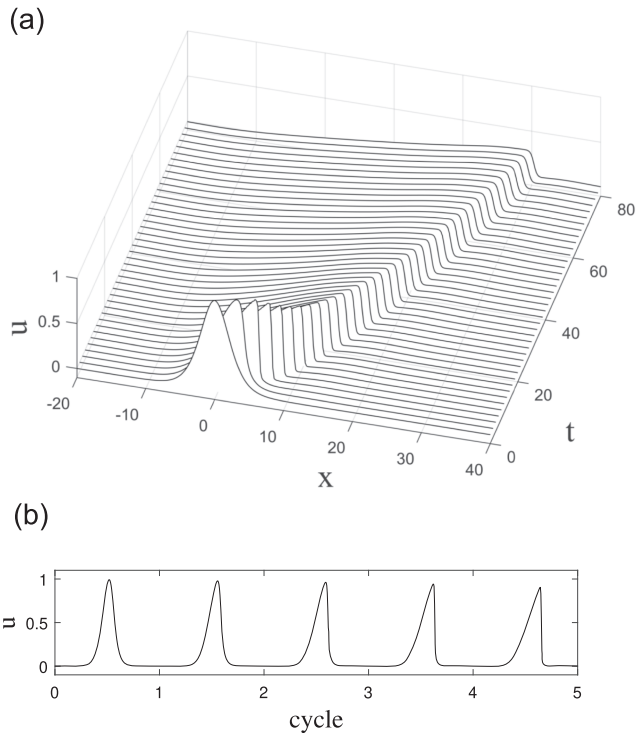

FIG. 8. Plots of the time evolution of Eq. (23), $\varepsilon = 0.05$ with kernel $K_\nu(x)$. The initial condition is given by Eq. (27). (a) $\nu = \frac{\pi}{8}$. Shocks occur. The nature of the solution is different to that in Fig. 7, and the wave breaks. (b) Line plot corresponding to the breaking wave in (a).

© Author(s) 2021

Results are presented in Fig. 6 as a series of line plots. For $\nu = \pi$, the solution is a continuous wave train that slowly decays. At $\nu = \frac{\pi}{4}$, shocks quickly appear and the solution decays.

The next example is the breaking of a solitary wave. The equation is (23) with $K_\nu(x)$ given by Eq. (11), $\varepsilon = 0.02$, and the initial condition is

$$u(x,0) = \operatorname{sech}^2 \frac{1}{2\sqrt{2}} x. \tag{27}$$

Then, for $\nu = \pi$, the solution is given in Fig. 7(a) where it is seen to be continuous for $0 \le t \le 80$. The line plot in Fig. 7(b) emphasizes the continuous nature of the exact soliton solution. When $\nu = \frac{\pi}{8}$, Fig. 8(a) shows that a shock occurs and the line plot [Fig. 8(b)] clearly shows the evolution of the vertical forward face. If $\nu = 0$ so that $K_\nu(x) = 0$, then the shallow water theory predicts that a shock occurs in ~3.3 s so that the dispersion has not significantly slowed down the shock formation.

IV. COMPARISON WITH SOLUTIONS TO PERIODICALLY FORCED KORTEWEG–DE VRIES EQUATION

Chester[27] analyzed the effects of frequency dispersion and boundary layer damping on the time-periodic response of resonantly excited shallow water waves in a tank of finite length. Chester and Bones[28] gave experimental results to validate Chester's steady state theory. Prior to that, Verhagen and van Wijngaarden[29] used the acoustic analogy with the polytropic constant $\gamma = 2$ to show that shallow water theory predicted shocks moving in a tank under resonant excitation; see Ref. 30 for the corresponding problem of a gas in a tube. In a band about the resonant frequency, the resonant band, Chester[27] showed that the waves produced in the tank are characterized by high peaks separated by low troughs; see Fig. 9 of Ref. 28 or Fig. 13 here. The evolution of such resonant solutions is given in Ref. 23 by analyzing a modified periodically forced KdV equation, and the predictions compare well with the numerical and experimental results in Ref. 28. We wish to examine here the effects of replacing the dispersion term in the KdV equation with the kernel $K_\nu(x)$, given by Eq. (11), as in Eq. (3), and in particular, we examine solutions around the resonant frequency. Then, it is shown how continuous solutions of the kernel equation evolve to shock solutions of shallow water theory by reducing ν.

The boundary layer damping in Eq. (28) is approximated by λu, where $\lambda \ll 1$. Chester[27] modeled the damping by means of a convolution integral $\frac{1}{4}\beta\int_{-\infty}^{\infty}(\operatorname{sgn} r + 1)\frac{\partial f_0}{\partial t}(t-r,\tau)|\pi r|^{-\frac{1}{2}}dr$; see Eq. (5.1) of Ref. 23. It was found in the latter that the simpler term λu maintains the same solution structure as (5.1) for small damping. The structure of the signal remains insensitive to the precise representation of the damping, and this is shown in Ref. 23, Figs. 3 and 5, where $\beta = 0.0287$ and $\lambda = 0.025$, respectively.

The kernel equation for the evolution of resonant oscillations in a tank has the form [see Ref. 23, Eq. (5.3)]

$$u_t - \frac{\delta^2}{6}\int_{-\infty}^{\infty} K_\nu(x-\xi)u_\xi(\xi,t)d\xi + \bar{\Delta}u_x - \frac{3}{2}\varepsilon u u_x + \lambda u - \bar{\varepsilon}u_{xx} = \pi\omega(1-\cos 2\pi\omega)\sin \pi x, \tag{28}$$

with the initial condition of rest

$$u(0,x) = 0, \tag{29}$$

and $\bar{\Delta} = 2\omega - 1$ is a detuning parameter, λu is a damping term that models boundary layer friction (see Ref. 23) and ensures convergence to a steady state, the Burgers term $\bar{\varepsilon}u_{xx}$ is included to structure shocks if they occur, $0 < \varepsilon, \bar{\varepsilon} \ll 1$, and the resonant frequency is $\bar{\Delta} = 0$ or $\omega = \frac{1}{2}$. In Figs. 9–12, $H = 3\varepsilon\omega u$.

A. Resonance at $\omega = \frac{1}{2}$, $\nu = 2\pi, \frac{\pi}{4}$

In Fig. 9, we show the continuous periodic output for the parameter values $\nu = 2\pi$, $\delta = 0.083$, $\bar{\Delta} = 0$, i.e., resonance, $\varepsilon = 0.002\,58$, $\lambda = 0.025$, $\bar{\varepsilon} = 0$. The waterfall plot in Fig. 9(a) shows a high peak per cycle, for $\nu = 2\pi$, with a low trough, while Fig. 9(b) shows the corresponding line plot, which can be compared with Fig. 5 of Ref. 23 or Fig. 13 here.

Now, we examine the case $\omega = \frac{1}{2}$, $\nu = \frac{\pi}{4}$ with the same values of the other parameters and $\bar{\varepsilon} = 0.001$. Figure 10 shows a discontinuous solution joined by part of a sine wave. The form of the solution compares well with the experimental result in Ref. 29 or Ref. 31 and the theoretical results in Ref. 30 or Ref. 32 where the factor $\frac{3}{2}$ is replaced by $\frac{\gamma+1}{2}$ in the case of a gas. This is the shallow water solution at resonance that contains a shock; see Ref. 29. See Ref. 34 for the evolution of resonant oscillations of a gas in a closed tube.

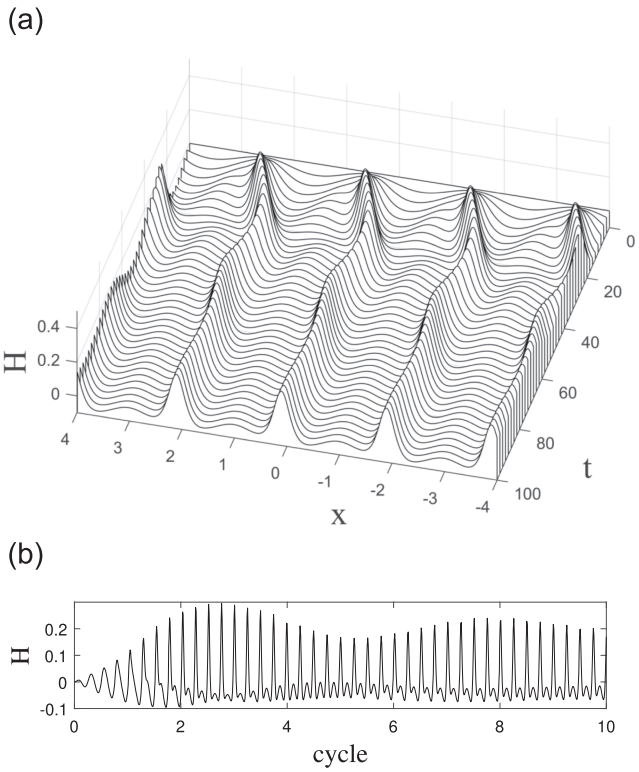

FIG. 9. Time evolution of Eqs. (28) and (29) using the kernel $K_\nu(x)$, $\bar{\varepsilon} = 0.0001$, and $\omega = 0.5$. (a) Waterfall plot for $\nu = 2\pi$. The solution is smooth and continuous. (b) Line plot corresponding to (a). This is the KdV solution at resonance.

© Author(s) 2021

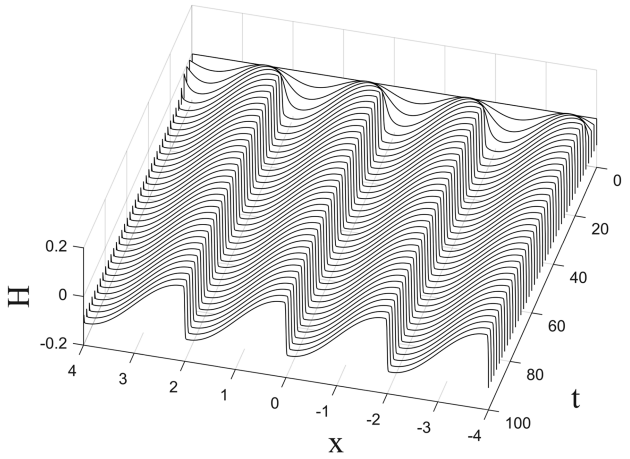

FIG. 10. Time evolution of resonant oscillations in Eqs. (28) and (29) using the kernel $K_\nu(x)$, $\bar{\varepsilon} = 0.0005$, and $\omega = 0.5$. Waterfall plot for $\nu = \frac{\pi}{4}$. The solution evolves to a shock corresponding to periodic resonance in a tank under shallow water theory.

B. Off-resonance at $\omega = 0.43$, $\nu = 2\pi$, $\frac{\pi}{4}$

The parameters here are $\delta = 0.083$, $\bar{\Delta} = -0.14$ or $\omega = 0.43$, $\varepsilon = 0.002\,58$, $\lambda = 0.025$, and the line plot shows $H = 3\varepsilon\omega u$ as a function of t.

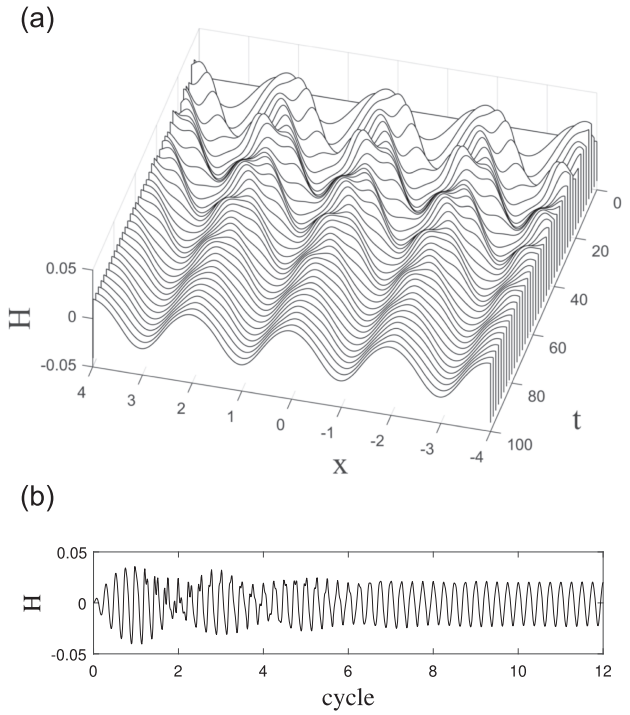

FIG. 11. Time evolution of off-resonance oscillations in Eqs. (28) and (29) using the kernel $K_\nu(x)$, $\bar{\varepsilon} = 0.0001$, and $\omega = 0.43$—off-resonance. (a) Waterfall plot for $\nu = 2\pi$. The solution is smooth and continuous and settles a periodic state. (b) Line plot corresponding to (a). This corresponds to the evolution of the kernel solution just outside the resonant band.

Figure 11(a) shows H for $0 \le t \le 100$, and the portion $0 \le t \le 25$ can be compared with the early part of Fig. 6 of Ref. 23. Then, Fig. 11(b) shows the steady state, with $50 \le t \le 100$, which is now settled to the linear periodic solution and is the response outside the resonant band. This may be compared with the last part of Fig. 6 of Ref. 23.

The situation when $\nu = \frac{\pi}{4}$ is shown in Fig. 12 and demonstrates that outside the resonant band, shock solutions do not occur in the shallow water theory. The resonant band in this case is defined as the range of frequencies for which shocks occur and has approximately the same width as that for the frequency dispersed equation. Figure 12 with $\nu = \frac{\pi}{4}$ and $\omega = 0.43$ should be compared with Fig. 10 with $\nu = \frac{\pi}{4}$ and $\omega = \frac{1}{2}$ and with Fig. 11 from cycle 8 onward. Outside the resonant band, the solutions for the dispersed equation and the shallow water equation both become sinusoidal. Note the similarity in the line plots in Figs. 11 and 12.

C. Convergence to the steady state

Following the time evolution of solutions to Eq. (28), for example, as shown in Figs. 9–11, indicates that the solutions tend toward a steady state. The steady state is found by solving the ordinary differential equation

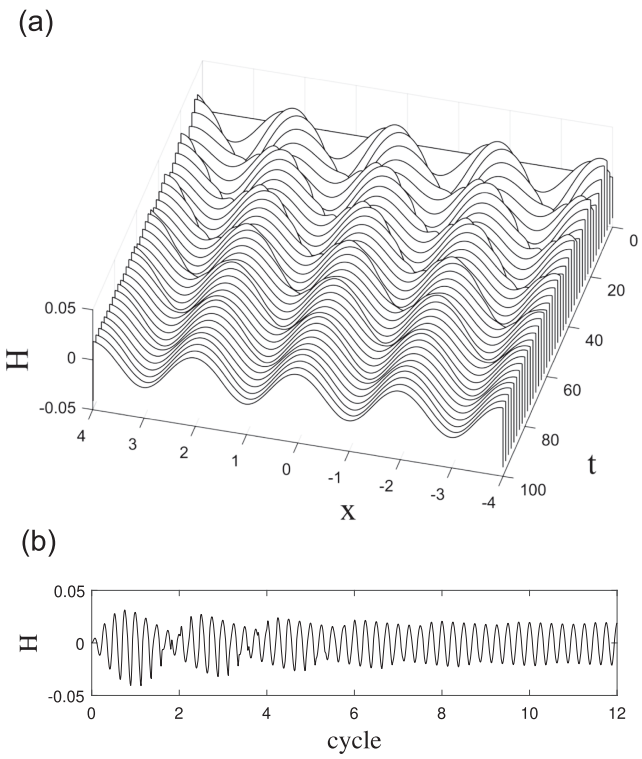

FIG. 12. Time evolution of off-resonance oscillations to Eqs. (28) and (29) using the kernel $K_\nu(x)$, $\bar{\varepsilon} = 0.0001$, and $\omega = 0.43$. (a) Waterfall plot for $\nu = \frac{\pi}{4}$. The solution is smooth and continuous and settles to a periodic state. (b) Line plot corresponding to (a). This corresponds to the shallow water solution just outside the resonant band, which settles to a sinusoidal state.

© Author(s) 2021

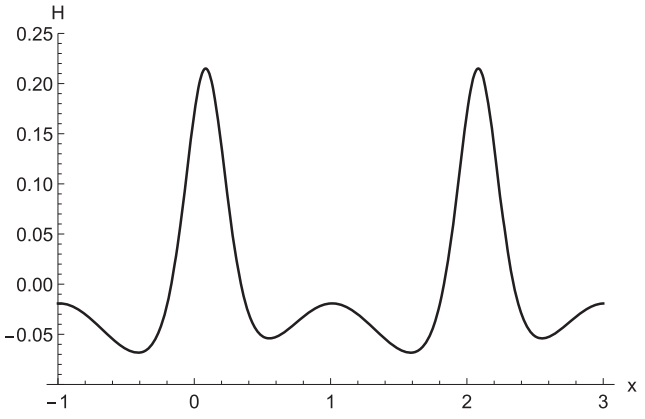

FIG. 13. Solution to Eq. (30) for $\omega = \frac{1}{2}$, $\delta = 0.083$, $\bar{\Delta} = 0$, $\varepsilon = 0.002\,58$, $\bar{\varepsilon} = 0$, and $\lambda = 0.025$ using a Fourier series approximation with 20 terms. $H = 3\varepsilon\omega u$. This is the resonant periodic oscillation.

$$-\frac{\delta^2}{6}u_{xxx} + \bar{\Delta}u_x - \frac{3}{2}\varepsilon u u_x + \lambda u - \bar{\varepsilon}u_{xx} = \pi\omega(1 - \cos\,2\,\pi\omega)\,\sin\,\pi x, \tag{30}$$

with the initial condition of rest

$$u(0, x) = 0 \tag{31}$$

using a standard Fourier analysis as briefly described in Sec. II B. An example steady state solution for resonance ($\bar{\Delta} = 0$) in a shallow water tank is shown in Fig. 13, which shows high peaks and low troughs.

Our question is does the solution to Eqs. (28) and (29) with kernel $K_\nu(x)$ converge to the steady state solution of the forced KdV equations (30) and (31). To answer this, we took solutions to the kernel equation (28) for $0 \le t \le 100$ for values around the resonant frequency $\omega = \frac{1}{2}$, $w = 0.5, 0.55, 0.45, 0.43$. Then, we calculated the least squares difference between the two, i.e., (28) and (30), as a function of time. The results are shown in Fig. 14. In each case, the least squares difference is reduced by 3 orders of magnitude between

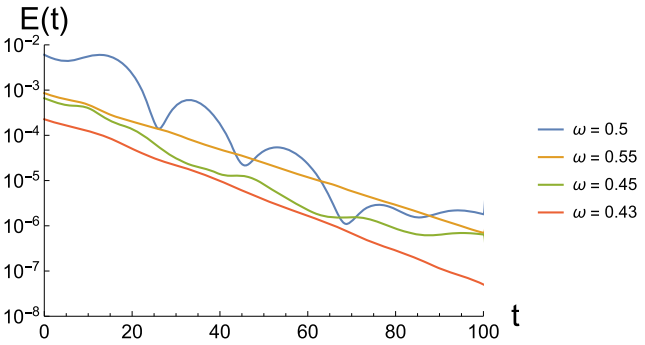

FIG. 14. Least squares difference [$E(t)$, see Eq. (20)] between solutions to Eq. (28) and the corresponding steady state solution of (30) for different values of ω. Parameter values are $\delta = 0.083$, $\varepsilon = 0.002\,58$, $\bar{\varepsilon} = 0.001$, and $\lambda = 0.025$.

$t = 0$ and $t = 100$. This indicates that the solutions to (28) converge to the steady state solution.

V. RESONANT PERIODIC SOLUTIONS OF A FORCED MODIFIED KdV EQUATION

In Figs. 2 and 3, Fornberg and Whitham[4] showed the interaction of two waves for the *modified KdV equation*,

$$u_t + 3u^2u_x + u_{xxx} = 0. \tag{32}$$

For resonance in a closed tube, the output depends on the quadratic nonlinearity in the equation of state, while in the case of an open tube, it depends on the cubic nonlinearity. Chester[39] gave the basic steady state equation (following scalings) for a Riemann invariant g of the nonlinear hyperbolic system governing the motion in an open tube as the cubic

$$g^3 + \frac{3r}{2^{2/3}}g + \sin\,\tau = 0. \tag{33}$$

Chester remarks that such a cubic is deducible from Refs. 36 and 37. The parameter r gives a measure of detuning from resonance, where $r = 0$ signifies resonance. The periodic output from Eq. (33) is given in Fig. 2 of Ref. 39.

The resonance of an ideal gas in a pipe, open at one end, has been studied analytically in a number of papers, such as by Seymour and Mortell,[36] Jimenez,[37] Keller,[38] Chester,[39] and Amundsen *et al.*[40] Experimental results can be found in the work of Sturtevant[41] and Stahlträger and Thoman.[42] Cox and Kluwick[43] analyzed resonant gas oscillations with mixed nonlinearity in a closed tube. By mixed nonlinearity, we mean that Eq. (32) contains terms such as uu_x and u^2u_x.

We want to study the forced *modified* kernel equation

$$0 = \cos\,x + g_t + 3g^2g_x + \lambda g_x + \int_{-\infty}^{\infty} K_\nu(x - \xi)u_\xi(\xi, t)d\xi. \tag{34}$$

For the steady state, $g_t = 0$, and with $K_\nu(x) = 0$, we integrate once to get Chester's basic equation (33), with $\lambda = \frac{3r}{2^{\frac{2}{3}}}$. For large ν, we expect resonant periodic solutions of (34), and for $\nu \to 0$, we expect to find solutions corresponding to (33) as displayed in Fig. 2 of Ref. 39.

The result of solving the evolution equation (34), subject to zero initial conditions is shown in Figs. 15 and 16. For $\nu = \pi$ in Fig. 15, we get continuous periodic solutions for five values around the resonant frequency at $r = 0$ when dispersion is dominant. For $\nu = \frac{\pi}{8}$ in Fig. 16, we recover the steady state solutions for resonance on an open tube in Fig. 2 of Ref. 39. The solution at resonance, $r = 0$, is continuous, while the solution at $r = -0.5$ has discontinuities of compression and rarefaction. Chester[39] explained why such solutions are physically realistic in this context of an open tube. The solution at $r = -1.0$ lies at the edge of the resonant band when the solution is continuous with a discontinuous slope. For $r < -1.0$ and $r \ge 0.5$, the oscillations begin to resemble sinusoidal profiles associated with linear acoustic oscillations. Two such examples are $r = 1.0$ and $r = -1.5$.

© Author(s) 2021

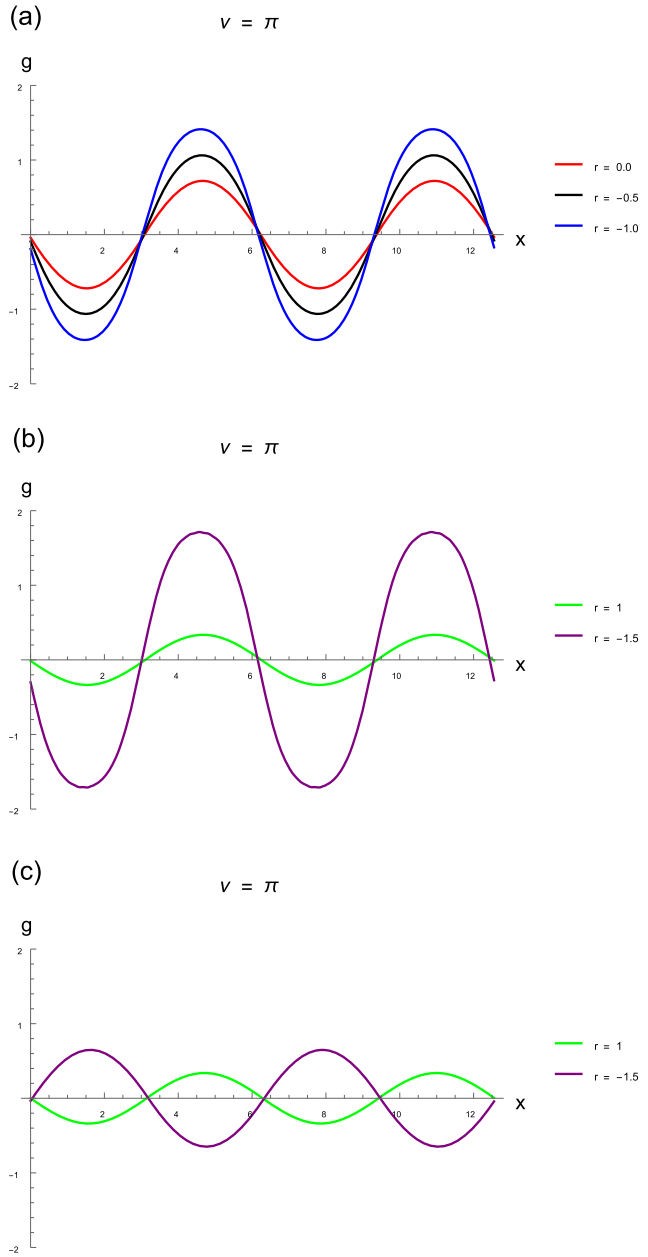

FIG. 15. Steady states for the open tube equation. [(a) and (b)] The equation solved is $g_t = -\cos x - 3g^2 g_x - \lambda g_x - \hat{\mu} g + \int_{-\infty}^{\infty} K_v(x-\xi) g_\xi(\xi,t)\,d\xi + \varepsilon g_{xx}$ with $\lambda = \frac{3r}{2^{\frac{2}{3}}}$, $\hat{\mu} = 0.025$, and $\varepsilon = 0.05$. The initial condition is $g(x,0) = 0$. (c) Same equation is solved but with initial condition $g(x,0) = 0.6 \sin x$.

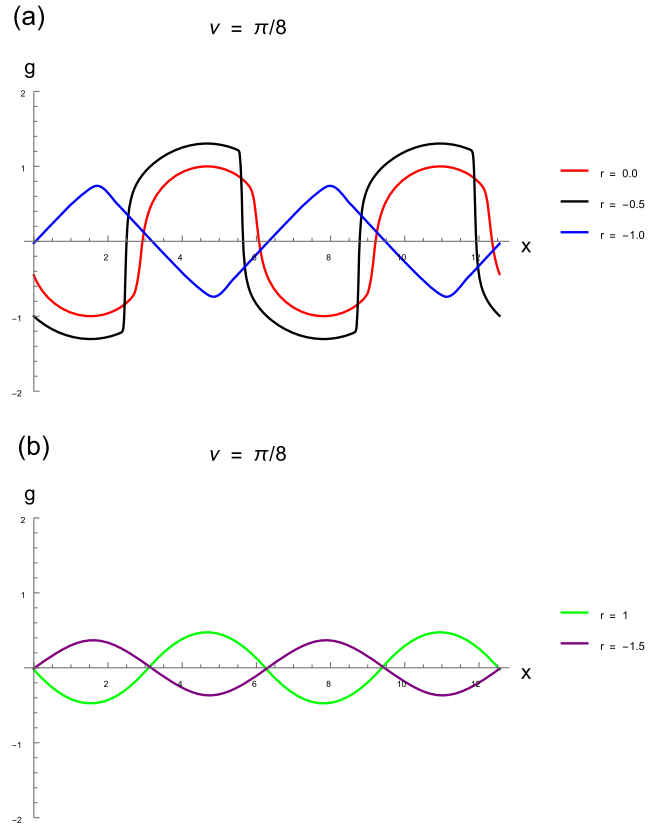

FIG. 16. Steady states for the open tube equation. [(a) and (b)] The equation solved is $g_t = -\cos x - 3g^2 g_x - \lambda g_x - \hat{\mu} g + \int_{-\infty}^{\infty} K_v(x-\xi) g_\xi(\xi,t)\,d\xi + \varepsilon g_{xx}$ with $\lambda = \frac{3r}{2^{\frac{2}{3}}}$, $\hat{\mu} = 0.025$, and $\varepsilon = 0.05$. The initial condition is $g(x,0) = 0$.

In Figs. 15 and 16, the initial condition is $g(x,0) = 0$. If the initial condition for $v = \pi$ is $g(x,0) = 0.6 \sin x$, then the graphs for $r = 0.0$, 0.5, and -1.0 match that in Fig. 15(a). However, the graph for $r = 1.0$ and $r = -1.5$ is affected by the change in initial condition and is given in Fig. 15(c). For $v = \frac{\pi}{8}$, with $g(x,0) = 0.6 \sin x$, the graphs match those in Fig. 16.

VI. A MATHEMATICAL MODEL FOR THE STRUCTURE OF "BORES"

Two forms of bores can result when the breaking of a wave occurs rather than peaking. An undular bore on the River Severn and a turbulent bore also on the River Severn are shown in Figs. 48 and 49 on pp. 181 and 182 in Ref. 33. The weaker bore, which is oscillatory in nature, is referred to as an "undular bore" (see Fig. 48 of Ref. 33), and the stronger bore, which has a weak wave train, is a "turbulent bore" (see Fig. 49 of Ref. 33). Favre's experimental results[35] give the critical value of the Froude number $F = \frac{u}{\sqrt{gh_1}} = 1.2$ at which the change in type occurs, and the depth ratio is $\frac{h_2}{h_1} = 1.28$. In the spirit of Whitham (Ref. 3, p. 482), "whatever the validity of the model may be," we ask whether the kernel equation (23), where $K(x) \equiv K_v(x)$ is given in (11), can, in some cases, contain both forms of bore shapes.

Whitham[3] provided the KdV as the natural starting place for an analysis, but it does not have the appropriately shaped solutions propagating unchanged, and so he added a second derivative dissipative term (like the Burgers term). The choice of the coefficient of this term then yields an oscillatory solution for small damping, while larger damping suppresses the oscillation; see Fig. 13.6 of Ref. 3.

© Author(s) 2021

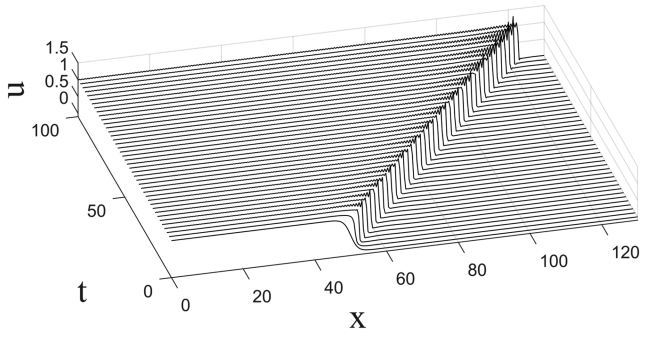

FIG. 17. Bore model with a hydraulic jump—a "turbulent bore." Solution to Eq. (23) with $K_\nu(x)$ given by Eq. (11) $\nu = \frac{\pi}{8}$ and $\varepsilon = 0.05$. The initial condition is given by Eq. (35).

We take Eq. (23) with $K_\nu(x)$ given by Eq. (11) as our starting point, with the initial condition

$$u(0,x) = A\left(\frac{1}{1+e^{\omega_1(x+a)}} - \frac{1}{1+e^{\omega_2(x+b)}}\right), \tag{35}$$

where A controls the height of the bore, and take $a > b$; then, a and b specify the positions where $u(0,x) = \frac{1}{2}A$, i.e., the position of the front and back of the bore, respectively. The parameters ω_1 and ω_2 determine the slope of the front and back of the bore, respectively. Ahead of the front and behind the back, $u(0,x)$ tends to zero. Spurious interactions between the back and front of the bore are mitigated by ensuring $A \ll a - b$, i.e., the initial bore is much wider than the bore height. In the following example, we take $A = 1$, $a = -50$, $b = 180$, $\omega_1 = 1$, and $\omega_2 = \frac{1}{4}$. We note that Eq. (23) with $K_\nu(x)$ given by Eq. (11) is just the kernel form of Whitham's starting point, Eq. (13.137), on which he comments "This may not be a very close model to the frictional effects in water waves, but is of interest in any case, since the Korteweg-de Vries equation is a canonical one for the general study of dispersive waves."

If we take $\nu = 2\pi$, we get approximate solutions of the corresponding KdV. In order to get discontinuous solutions to Eqs. (23) and (35), we reduce ν to $\frac{\pi}{8}$ and thus significantly increase the role of the nonlinear shallow water term. The result is shown in Fig. 17, which resembles a turbulent bore or a hydraulic jump.

Since the undular bore is weaker than the turbulent bore, we increase ν to $\nu = \frac{3\pi}{8}$, which gives more effect to the frequency dispersion embedded in Eq. (23) and a different balance between dispersion and nonlinearity. The result is shown in Fig. 18, which resembles an undular bore. It is worth noting that the difference between Figs. 17 and 18 depends only on the relative influence of dispersion and nonlinearity in Eq. (23) since only the value of the parameter ν has changed.

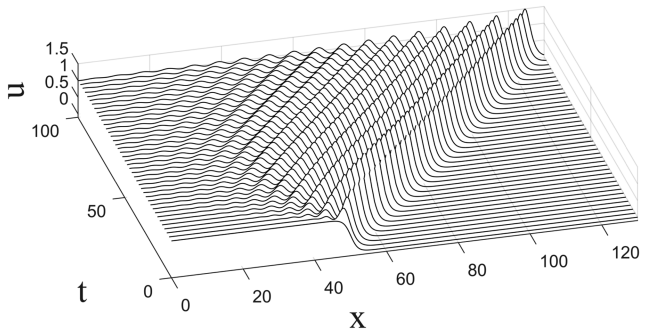

FIG. 18. Bore model with a following wave train—an "undular bore." Solution to Eq. (23) with $K_\nu(x)$ given by Eq. (11), $\nu = \frac{3\pi}{8}$, and $\varepsilon = 0.05$. The initial condition is given by Eq. (35).

VII. CONCLUSION

The purpose of this paper was to construct a simple Whitham type equation that contains both continuous solutions and shocks that correspond to breaking due to nonlinear hyperbolicity. The motivation was the widely used observation, including Whitham,[3] that the KdV does not have shocks, while shallow water theory has only shocks for an initial increase in elevation. We numerically examine equations of the form (17), (23), (28), (30), and (34) where we have used the kernel given by (11). In all cases, the KdV results are found for $\nu \gg 1$ and shallow water results are found for $\nu \ll 1$ from the kernel equation.

ACKNOWLEDGMENTS

We would like to thank Professor Nhan Phan-Thien for editorial assistance and the anonymous reviewers who helped improve the manuscript.

DATA AVAILABILITY

The data that support the findings of this study are available from the corresponding author upon reasonable request.

REFERENCES

[1] J. S. Russell, "Report on waves," in *14th Meeting of the British Association Report, York* (British Association Report, 1844), pp. 311–390.
[2] M. K. Brun and H. Kalisch, "Convective wave breaking in the KdV equation," Anal. Math. Phys. **8**, 57–75 (2018).
[3] G. B. Whitham, *Linear and Nonlinear Waves* (John Wiley & Sons, New York, 1974), p. 636.
[4] B. Fornberg and G. B. Whitham, "A numerical and theoretical study of certain nonlinear wave phenomena," Philos. Trans. R. Soc., A **289**, 373–404 (1978).
[5] R. L. Seliger, "A note on the breaking of waves," Philos. Trans. R. Soc., A **303**, 493–496 (1968).
[6] A. Constantin and J. Escher, "Wave breaking for nonlinear nonlocal shallow water equations," Acta Math. **181**, 229–243 (1998).
[7] This paragraph is based on an anonymous private communication, for which we are most grateful.
[8] M. Ehrnström and H. Kalisch, "Traveling waves for the Whitham equation," Differ. Integr. Equations **22**, 1193–1210 (2009).
[9] M. Ehrnström, M. D. Groves, and E. Wahlén, "On the existence and stability of solitary-wave solutions to a class of evolution equations of Whitham type," Nonlinearity **25**, 2903–2936 (2012).
[10] N. Sanford, K. Kodama, J. D. Carter, and H. Kalisch, "Stability of traveling wave solutions to the Whitham equation," Phys. Lett. A **378**, 2100–2107 (2014).
[11] D. Moldabayev, H. Kalisch, and D. Dutykh, "The Whitham Equation as a model for surface water waves," Physica D **309**, 99–107 (2015).

© Author(s) 2021

[12]V. M. Hur and M. A. Johnson, "Modulational instability in the Whitham equation for water waves," Stud. Appl. Math. **134**, 120–143 (2015).
[13]J. D. Carter, "Bidirectional Whitham equations as models of waves on shallow water," Wave Motion **82**, 51–61 (2018).
[14]J. L. Hammack and H. Segur, "The Korteweg-de Vries equation and water waves. Part 3. Oscillatory waves," J. Fluid Mech. **84**, 337–358 (1978).
[15]V. M. Hur, "Wave breaking in the Whitham equation," Adv. Math. **317**, 410–437 (2017).
[16]V. M. Hur and L. Tao, "Wave breaking in a shallow water model," SIAM J. Math. Anal. **50**, 354–380 (2018).
[17]M. Ehrnström and E. Wahlén, "On Whitham's conjecture of a highest cusped wave for a nonlocal dispersive equation," Ann. l'Inst. Henri Poincare C **36**, 1603–1637 (2019).
[18]H. Borluk, H. Kalisch, and D. P. Nicholls, "A numerical study of the Whitham equation as a model for steady surface water waves," J. Comput. Appl. Math. **296**, 293–302 (2016).
[19]J. R. Dormand and P. J. Prince, "A family of embedded Runge-Kutta formulae," J. Comput. Appl. Math. **6**, 19–26 (1980).
[20]M. J. Lighthill, *Fourier Analysis and Generalised Functions* (Cambridge University Press, Cambridge, 1958), p. 79.
[21]A. Erdélyi, *Operational Calculus and Generalized Functions* (Holt, Rhinehart and Winston, New York, 1962), p. 103.
[22]G. B. Whitham, "Variational methods and applications to water waves," Proc. R. Soc. London, Ser. A **299**, 6–25 (1967).
[23]E. A. Cox and M. P. Mortell, "The evolution of resonant water-wave oscillations," J. Fluid Mech. **162**, 99–116 (1986).
[24]B. Fornberg, *A Practical Guide to Pseudospectral Methods* (Cambridge University Press, Cambridge, 1998), p. 231.
[25]L. N. Tefethen, *Spectral Methods in MATLAB (Software, Environment and Tools)* (SIAM, Philadelphia, PA, 2000), p. 183.
[26]M. P. Mortell and B. R. Seymour, *Nonlinear Waves in Bounded Media* (World Scientific, 2017), p. 405.
[27]W. Chester, "Resonant oscillations of water waves. I. Theory," Philos. Trans. R. Soc., A **306**, 5–22 (1968).
[28]W. Chester and J. A. Bones, "Resonant oscillations of water waves. II. Experiment," Philos. Trans. R. Soc., A **306**, 23–39 (1968).
[29]J. H. G. Verhagen and L. van Wijngaarden, "Nonlinear oscillations of fluid in a container," J. Fluid Mech. **22**, 737–752 (1965).
[30]W. Chester, "Resonant oscillations in closed tubes," J. Fluid Mech. **18**, 44–64 (1964).
[31]R. A. Saenger and G. E. Hudson, "Periodic shock waves in resonating gas columns," J. Acoust. Soc. Am. **32**, 961–970 (1960).
[32]B. R. Seymour and M. P. Mortell, "Resonant acoustic oscillations with damping: Small rate theory," J. Fluid Mech. **58**, 353–373 (1973).
[33]M. J. Lighthill, *Waves in Fluids* (Cambridge University Press, 1978), p. 504.
[34]E. A. Cox and M. P. Mortell, "The evolution of resonant oscillations in closed tubes," Z. Angew. Math. Phys. **34**, 845–866 (1983).
[35]H. Farvre, *Etude Théorique et Expérimentale des Ondes de Tanslation dans les Canaux Decouverts* (Duriod et Cie, Paris, 1932).
[36]B. R. Seymour and M. P. Mortell, "Nonlinear resonant oscillations in open tubes," J. Fluid Mech. **60**, 733–750 (1973).
[37]J. Jimenez, "Nonlinear gas oscillations in pipes. Part 1. Theory," J. Fluid Mech. **59**, 23–46 (1973).
[38]J. J. Keller, "Resonant oscillations in open tubes," Z. Angew. Math. Phys. **28**, 237–263 (1977).
[39]W. Chester, "Resonant oscillations of a gas in an open-ended tube," Philos. Trans. R. Soc., A **377**, 449–467 (1981).
[40]D. E. Admundsen, M. P. Mortell, and B. R. Seymour, "Resonant oscillations in open axisymmetric tubes," Z. Angew. Math. Phys. **68**, 139 (2017).
[41]B. Sturtevant, "Nonlinear gas oscillations in pipes. Part 2. Experiment," J. Fluid Mech. **63**, 97–120 (1974).
[42]E. Stuhlträger and H. Thoman, "Oscillations of a gas in an open-ended tube near resonance," Z. Angew. Math. Phys. **37**, 155–175 (1986).
[43]E. A. Cox and A. Kluwick, "Resonant gas oscillations exhibiting mixed nonlinearity," J. Fluid Mech. **318**, 251–271 (1996).

© Author(s) 2021